- Technical Paper -

COMPARISON OF SPH AND MPS METHODS FOR NUMERICAL FLOW SIMULATIONS OF FRESH MORTAR

Zhisong XU[*1], Zhuguo LI[*2], Guodong CAO[*3] , Fei JIANG[*4]

ABSTRACT

This paper aims to compare the accuracy of weakly compressive SPH and MPS methods for the flow simulation of fresh cementitious materials, and to clarify their application scope. By comparing the numerical and experimental results of L-flow test of three series of fresh mortars with different fluidity, it was concluded that MPS has higher efficiency and accuracy than SPH. SPH is relatively suitable for fresh mortar with low fluidity, whereas MPS is applicable to any mortar if boundary resistance is certainly considered. The boundary resistance greatly affects the simulation result and accuracy.

Key works: SPH, MPS, Fresh Mortar, L-box test

1. INTRODUCTION

As an important property of fresh concrete, workability seriously affects the construction efficiency and quality of concrete. Large-scale construction experiments require a lot of time, materials and labor costs. The importance of workability evaluation and design based on numerical flow simulations has been gradually recognized because of their high efficiency and environmental friendliness. The flow of fresh concrete is a large deformation problem with a free surface. Hence, meshless particle methods, such as SPH (Smoothed Particle Hydrodynamics) and MPS (Moving Particle Semi-Implicit), are commonly used for the flow simulation of fresh concrete.

SPH was originally used to solve compressible hydrodynamic problem in astrophysics[1]. Later, Monaghan[2] used WCSPH (Weakly Compressible SPH) to solve the incompressible flow problem by introducing a weakly compressible model. On the other hand, for analyzing incompressible fluid problem, Koshizuka[3] developed a kind of new meshless method called MPS in 1996.

There are differences between SPH and MPS methods. Mainly, the particles are weakly compressible in SPH but incompressible in MPS. there are many examples of flow simulation for fresh concrete, using SPH method[4],[5] and MPS method[6],[7]. In these numerical analyses, different boundary conditions were adopted, and the agreement degree between the numerical and experimental results was not assessed quantitatively though the numerical and experimental results were compared. Thus, it is unknown that which method is more applied to the numerical analysis of fresh cementitious materials.

In this paper, a series of flow simulations of three fresh mortars were performed by both SPH and MPS to clarify which method is more applicable to fresh mortar. And the effects of the fluidity and boundary resistance condition on the precisions of two numerical methods were discussed.

2. SPH AND MPS METHODS

2.1 Governing Equations

For both SPH and MPS method, the governing equations are the continuity equation and momentum equation, as shown in Eq.(1). The former describes the change of particles' density with time, the latter expresses the motion of particles depending on pressure, viscosity and gravity.

$$\frac{1}{\rho}\frac{D\rho}{Dt}+\nabla\cdot\vec{u}=0;\ \frac{D\vec{u}}{Dt}=-\frac{1}{\rho}\nabla P+\upsilon\nabla^2\vec{u}+\vec{g} \qquad (1)$$

where, ρ is the density of fluid particle, $\boldsymbol{u}$ is velocity of particles, t is time, P is pressure, v is kinematic viscosity of fluid, $\boldsymbol{g}$ is gravitational acceleration, and v is kinematic viscosity of fluid, which is a ratio of μ to ρ.

2.2 Main Differences Between SPH And MPS

In SPH and MPS, the discrete forms of governing equation are different. The main discrete equations used in SPH and MPS are summarized in **Table 1**.

(1) The kernel function in MPS functions as a weight function, whereas in SPH, it is not only used as a weight function, but also its derivative is used to calculate the differential operator such as a gradient.

(2) The density ρ in SPH is obtained by weight-averaging of the densities of all particles in each influential domain. In MPS, particle number density n is used instead of particle density, as particle density is a constant.

(3) When calculating viscosity force and pressure, SPH uses highly efficient explicit algorithm and state equation, but time-step is limited by the sound speed. MPS employs a time-consuming implicit algorithm and Poisson equation, which allows MPS method to set a large time-step.

*1 Graduate Student, Graduate School of Sci. & Tech. for Innovation, Yamaguchi University, JCI Member
*2 Prof. Graduate School of Sci. & Tech. for Innovation, Yamaguchi University, JCI Member
*3 Dr., Graduate School of Sci. & Tech. for Innovation, Yamaguchi University, JCI Member
*4 Assistant Prof., Department of Mechanical Engineering, Yamaguchi University

Table 1 Main differences between SPH and MPS

Item	SPH	Eq.	MPS	Eq.
Kernel function	$W(r,h)=\begin{cases}\frac{10}{7\pi h^2}\left(1-\frac{3}{2}q^2+\frac{3}{4}q^3\right) & 0\le q\le 1\\ \frac{10}{28\pi h^2}(2-q)^3 & 1\le q\le 2\\ 0 & q\ge 2\end{cases}, \quad q=\frac{r}{h}$	(2)	$w(r)=\begin{cases}\frac{r_e}{r_{ij}}-1, & 0<r_{ij}<r_e\\ 0, & r_{ij}\ge r_e\end{cases}; \ r_{ij}=\lvert\vec{r}_j-\vec{r}_i\rvert$	(3)
Particle density	$\frac{d\rho_i}{dt}=\sum_{j\ne i}m_j\vec{u}_{ij}\cdot\nabla_i W(r,h);\ \vec{u}_{ij}=\vec{u}_i-\vec{u}_j$	(4)	$\frac{dn_i}{dt}=\frac{1}{n_0}\sum_{j\ne i}\frac{-r_e}{r_{ij}^3}(\vec{r}_{ij}\cdot\vec{u}_{ij})$	(5)
Viscosity term	$\langle\upsilon\nabla^2\vec{u}\rangle_i=-\sum_{j\ne i}m_j\left[\frac{4\upsilon\vec{r}_{ij}\vec{u}_{ij}}{(\rho_i+\rho_j)\lvert\vec{r}_{ij}\rvert^2}\right]\nabla_i W(r,h)$	(6)	$\langle\upsilon\nabla^2\vec{u}\rangle_i=\frac{2d}{\lambda n_0}\sum_{j\ne i}\left[\frac{4\mu_i\mu_j}{(\mu_i+\mu_j)(\rho_i+\rho_j)}\vec{u}_{ij}w(r)\right]\quad\lambda=\frac{\sum_{j\ne i}\left[w(r)\cdot\lvert\vec{r}_{ij}\rvert^2\right]}{\sum_{j\ne i}w(r)}$	(7)
Pressure calculation	$P=B\left[\left(\frac{\rho}{\rho_0}\right)^{\gamma}-1\right]$	(8)	$\frac{2}{n_0}\sum_{j\ne i}\left[\frac{r_e}{\lvert\vec{r}_j^*-\vec{r}_i^*\rvert^3}(P_j-P_i)\right]=\frac{1}{n_0}\left(\frac{Dn}{Dt}\right)_i^*$	(9)
Pressure term	$\left(-\frac{1}{\rho}\nabla P\right)_i=-\sum_j m_j\left(\frac{P_i}{\rho_i^2}+\frac{P_j}{\rho_j^2}\right)\nabla_i W_{ij}$	(10)	$\langle\nabla P\rangle_i^{t+1}=\frac{2}{n_0}\sum_{j\ne i}\left[\frac{\hat{P}_j^{t+1}-\hat{P}_i^{t+1}}{\lvert\vec{r}_j^*-\vec{r}_i^*\rvert^2}(\vec{r}_j^*-\vec{r}_i^*)w(\lvert\vec{r}_j^*-\vec{r}_i^*\rvert)\right]$	(11)

Notes: r_{ij} : distance between two particles, h : smoothing length, r_e : radius of influence area, m_j : mass of particle j, d : model dimension (here, d is equal to 3), ρ_0 : initial density of fluid, $B=\rho_0 c_0^2/\gamma$, γ : a constant and equals to 7, c_0 : sound speed at the initial density ($c_0=c(\rho_0)=\sqrt{(\partial P/\partial\rho)}\,|_{\rho_0}$), and * indicates the temporary values of the variables after considering physical force and viscous force.

3. RHEOLOGICAL MODEL

At present the Bingham model is generally used to describe the flow behaviors of fresh concrete, especially it is applied to flowing concrete. The effective viscosity μ of fresh concrete or mortar for numerical computation are represented as:

$$\mu=\mu_b+\frac{\tau_0}{\dot{\gamma}} \tag{12}$$

where, τ_0 is yield stress, μ_b is plastic viscosity, and $\dot{\gamma}$ is shear strain rate that is defined by the second invariant of the deformation strain as:

$$\dot{\gamma}=\sqrt{2\mathrm{II}_D};\ \mathrm{II}_D=\frac{1}{2}D:D;\ D=\frac{1}{2}\left[(\nabla\vec{u})+(\nabla\vec{u})^T\right] \tag{13}$$

where, D is deformation rate tensor, II_D is the second invariant of D.

But when shear stress τ approaches to the yield stress τ_0, the constitutive law shown above is discontinuous so that the effective viscosity attains an infinite value, which leads to a numerical divergence in numerical computation. Hence, a regularized Bingham model[8] is used as shown in Eq.(14) and illustrated in **Fig. 1.**

$$\mu=\mu_b+\tau_0\frac{1-e^{\beta\dot{\gamma}}}{\dot{\gamma}} \tag{14}$$

where, β is a parameter related to the transition between the solid and fluid regimes. The larger the β, the sharper the transition.

4. BOUNDARY RESISTANCE

In both SPH and MPS, the boundary particles interact with the fluid particles within a spherical domain (r_e), as shown in **Fig. 2**, of which the radius was set as 2.1 times of particle center distance. In MPS, the radius of spherical domain was set as 4.1 times of particle center distance when calculating Laplacian operator.

The flow behavior of fresh mortar is also dependent on boundary resistance besides shear deformation resistance of itself. Meanwhile, it is adequate to regard fresh mortar as a Bingham fluid unless it is very dry. Murata et al.[7]'s experimental results showed that the boundary resistance of fresh concrete is linear function of flow velocity and has a minimum value that is similar to the yield stress of Bingham model. In this study, we proposed a boundary resistance model, as shown in Eq.(15), to describe the boundary slippage resistance of fresh mortar. The form of Eq.(15) is the same to that of Bingham model equation.

$$\tau_s=\tau_{s0}+\mu_{sb}\cdot\dot{\gamma} \tag{15}$$

where, τ_{s0} and μ_{sb} are yield stress and plastic viscosity of slippage between fresh mortar and boundary, respectively.

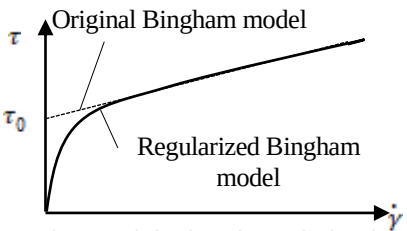

Fig. 1 Original and regularized Bingham models

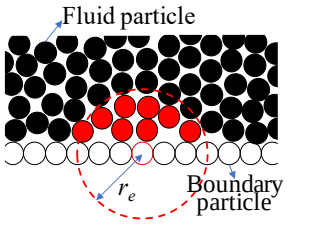

Fig. 2 Boundary influence area

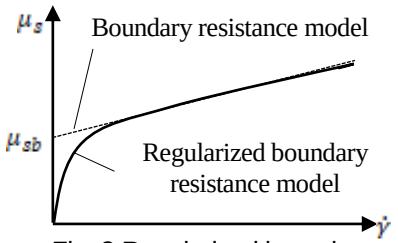

Fig. 3 Regularized boundary resistance model

Table 2 Mix proportions of fresh mortars and rheological parameters

Series No.	W/C	WR/C (%)	Unit mass (kg/m³)				Flow (mm)	Bingham model		Boundary Model	
			W	C	S	WR		τ_0 (Pa)	μ_b (Pa·s)	τ_{s0} (Pa)	μ_{sb} (Pa·s)
1	0.50	0.5	254.6	509.2	1273	2.5	102	1589.4	1337.8	19.9	16.7
2	0.55		280.1				159	498.2	425.8	6.2	5.3
3	0.60		305.5				200	365.9	235.4	4.6	2.9

Notes: *W/C*: water-cement ratio, *W*: water, *C*: cement, *S*: sand, *WR*: water reducing agent, τ_0: yield stress of fresh mortar, μ_b: plastic viscosity of fresh mortar, τ_{s0}: yield stress of boundary slippage, μ_{sb}: viscosity of boundary slippage, *Flow*: Flow table value with zero time dropping.

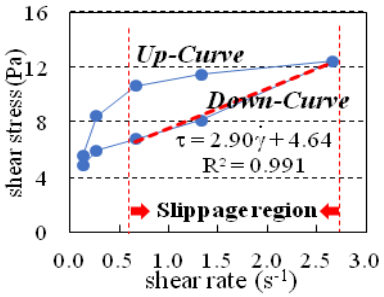

Fig. 4 Measure method of boundary constants (Series No.3)

A regularized method like the regularized Bingham model was used to avoid the numerical divergence, as shown in Eq.(16) and **Fig. 3**.

$$\mu_s = \mu_{sb} + \tau_{s0}\frac{1-e^{\beta\dot{\gamma}}}{\dot{\gamma}} \tag{16}$$

5. EXPERIMENT

5.1 Raw Materials And Mixtures

Ordinary Portland cement with specific surface area of 3500 cm²/g and density of 3.16 g/cm³ was used. Fine aggregate was sea sand with 2570 kg/m³ of density in saturated surface dry state, 1.36% of water absorption ratio, and 2.9 of fineness modulus. As bleeding would worsen the uniformity of mortar and further affect its rheological properties, AE water reducing agent was added to reduce water content and bleeding, and to improve fluidity of fresh mortars. Mix proportions of threes series of mortars are presented in **Table 2**. Their apparent densities were 2039 kg/m³, 2064 kg/m³ and 2090 kg/m³, respectively.

After the raw materials were prepared, cement and sand were first put into a mortar mixer, and mixed at speed of 48 rpm for 1 min. Then water and admixture were added and further mixed for 1 min. at speed of 48 rpm, and for another 1 min. at 64 rpm.

Right after mixing, Bingham constants were measured by the RSNS rheometer, and L-flow test was performed. The rotational speed of the rheometer was first increased with an angular acceleration of 5deg./s, then gradually reduced once the rotational speed reached 45 deg./s. The deceleration phase was used to calculate the Bingham constants. The intercept of the line was τ_0 and the slope was μ_b. The detailed measurement and calculation methods of τ_0 and μ_b can be found in Reference [6].

B-type viscometer is originally designed to measure the yield stress and viscosity of fluid, supposing that no slippage occurs between sample and rotor. However, for granular materials, the occurrence of slippage can't be avoided when rotating speed of rotor is large. Take Series No.3 as an example, as shown in **Fig. 4**. The rotor speed was first increased and then decreased to obtain the up-curve and down-curve of shear stress -shear rate relationship. In the increasing stage of shear rate, when shear rate was beyond 0.6s^{-1}, shear stress's increase was very small, the slope of up-curve suddenly decreased. This is usually considered to be due to the breakdown of flocculate structure of particles. However, if there weren't slippage, even if the flocculate structure was broken down, shear stress would largely increase with shear rate because fresh mortar has large viscosity. Hence, we consider that when rotating speed is high, the slippage occurs. Moreover, there is no other reasonable test method for slippage resistance now.

Thus, in this study, we employed a B-type viscometer to measure the constants of the boundary resistance model. The flocculate structure of particles may affect the magnitude of slippage resistance. Hence, the down-curve in the slippage region was used to calculate the constants τ_{s0}, μ_{sb} of the boundary resistance model. The intercept and the slope of the regressive line of down-curve were τ_{s0} and μ_{sb}, respectively.

Measured Bingham constants and Boundary constants are shown in **Table 2**. It should be noted that we investigated the difference in the accuracy of MPS and SPH, using the same values of material and boundary parameter for a given mortar sample, even if there are errors in these measurements, the conclusions obtained later are not affected.

5.2 L-Flow Test

The geometry of L-box used in the L-flow test is shown in **Fig. 5**. The height and section of vertical room for filling mortar sample was 25cm and 12 × 10cm, respectively, and the length of horizontal part was 60cm.

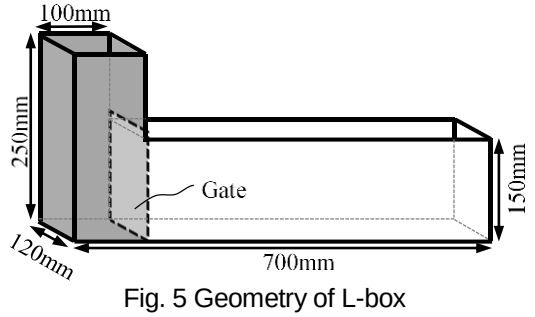

Fig. 5 Geometry of L-box

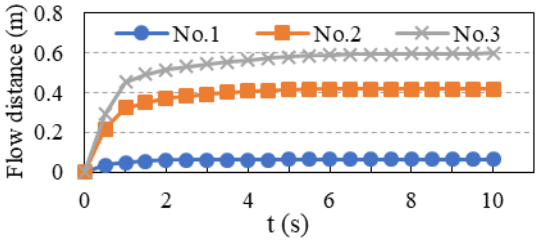

Fig. 6 Experimental results of L-flow distance-time relationship

Fig. 7 Final L-flow shapes of three series of mortars

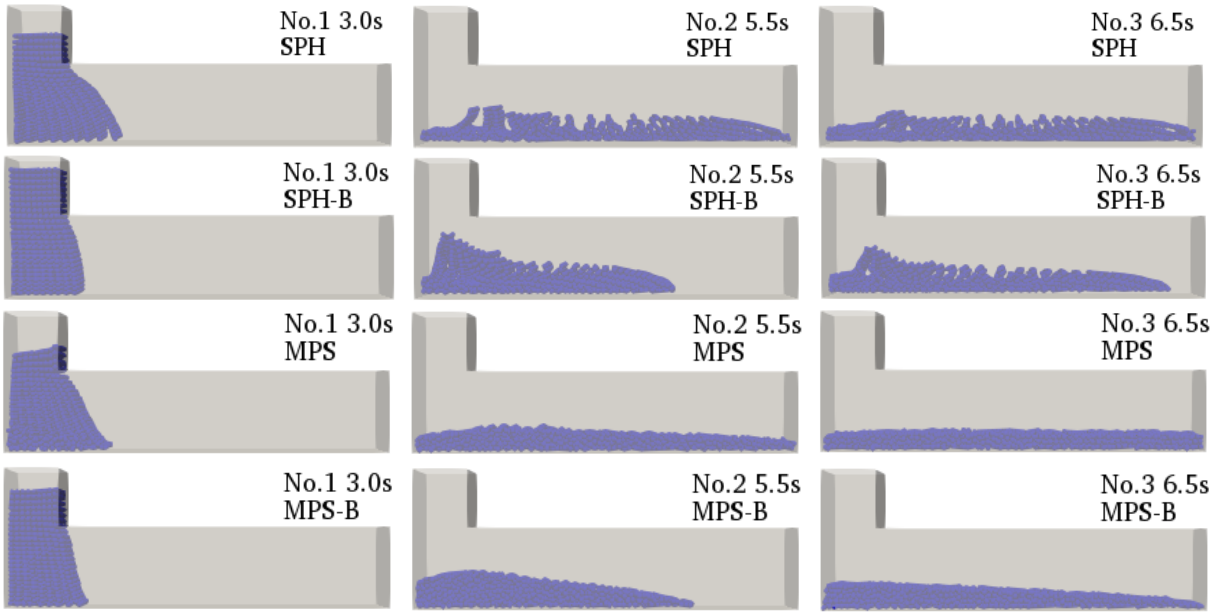

Fig. 8 Final L-flow shapes of numerical simulation

A scale with 1 mm of interval was attached to the L-box bottom.

Fresh mortar was cast into the vertical room of the L-box right after mixing, then the sliding gate was quickly lifted upward to allow the mortar to flow under its own weight. After the gate was opened, the flow distance of mortar was recorded by a video camera. L-flow distance-time relational curves were drawn in **Fig. 6**.The final flow shapes of the mortars in the L-box are shown in **Fig. 7**.

Series No.1, which had the smallest flow table value, flowed for 3.0 seconds till stop, and had the shortest flow distance of only 0.063m. Series No.2 flowed 0.419m and stopped at 5.5 seconds. Series No.3 had the highest fluidity and the flow did not stop until it reached the end of the horizontal part of L-box after 6.5 seconds.

6. NUMERICAL RESULTS AND DISCUSSION

6.1 Analytical Model

Sphere particles were used to represent fresh mortar and flow boundary, i.e. the L-box. Particle number of each mortar sample was 2475. In SPH, the L-box boundary was expressed by one layer of particles, of which the particle number was 3834. But in MPS, three layers of particles, which were 13156, were used to form the L-box boundary in order to ensure the accuracy of particle density. The particle center distance was set to be 10mm.

The time-step of SPH was dependent on the Courant-Friedrichs-Lewy (CFL) condition, the force term, and the viscous diffusion term. A variable time-step Δt is calculated by Eqs.(17)~(19).

$$\Delta t_f = \min\left(\sqrt{h/|f_i|}\right) \tag{17}$$

$$\Delta t_{cv} = \min \frac{h}{c_s + \max\left|\frac{h\vec{v}_{ij}\cdot\vec{r}_{ij}}{\vec{r}_{ij}^{\,2}}\right|} \tag{18}$$

$$\Delta t = 0.1\cdot\min\left(\Delta t_f, \Delta t_{cv}\right) \tag{19}$$

where, Δt_f is based on the force per unit mass $|f_i|$, and Δt_{cv} combines the Courant and the viscous time step, i and j represent the particles' number.

The SPH used an explicit algorithm to calculate particle motion, the calculation time-step Δt was variable. To prevent excessive accumulation or escape of particles, the Δt was set to be small, of which initial value was 0.00005s. However, since MPS uses an implicit algorithm, the Δt is a constant, and large calculation time-step can be used. The Δt was 0.001s in this study.

6.2 Comparison of Calculation Time

During the L-flow test, flow velocity of mortar gradually decreased with the elapsed time, and eventually became zero. However, in numerical simulation, the particle's velocity becomes smaller and smaller, but it never reaches zero[5]. Because the start and the stop of flow is dependent on yield stress, it was supposed that when the velocity reduced to $0.05\tau_0/\rho$, the particles came to stop, and the numerical calculation was stopped. The time consuming of each simulation was shown in **Fig. 9**. The numerical results of SPH and MPS in **Fig. 9** didn't consider the L-box boundary resistance, whereas the results of SPH-B and MPS-B took the boundary resistance into account by using Eq.(16).

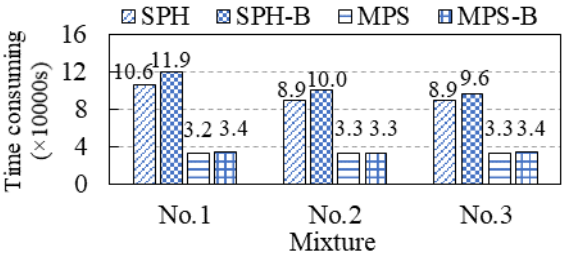

Fig. 9 Calculation times of different simulation methods

As shown in **Fig. 9**, for analyzing the same L-flow problem, compared to MPS method, SPH method required a longer time, no matter whether the boundary resistance was considered or not, and no matter how low the fluidity of mortar. This is because that MPS used the implicit algorithm so that larger time-step could be set than that of SPH though much time needed to solve the Poisson equation. Large time-step has the advantage of improving calculation efficiency.

Also, since the time-step in MPS was fixed, the time consumptions of simulation for different mortars and boundary conditions were almost the same. But in SPH, the time-step was determined on basis of the effective viscosity that changed with the fluidity of mortar. The lower the fluidity, the higher the effective viscosity. Higher viscosity leaded to a smaller time-step. Moreover, the consideration of boundary resistance would increase effective viscosity according to Eqs.(6) and (7). Hence, the calculating time of SPH-B simulation was longer than that of SPH simulation, and the simulation of series No.1, which had the lowest fluidity, took the longest time among three series.

6.3 Comparison of Calculation Accuracy

In order to clarify calculation accuracy's difference of SPH and MPS, the results of L-flow simulations of three series of fresh mortar using SPH and MPS, with and without considering boundary resistance, are compared to the experimental results, as shown in **Fig. 10** and **Fig. 11,** respectively.

According to these figures, calculation accuracy of SPH and MPS varies with boundary condition considered and mortar mixtures. For clearing up the calculation accuracy of SPH and MPS, boundary condition and analyzed material characteristic should be taken into account.

6.3.1 Influence of boundary condition on the difference of calculation accuracy

We compared the experimental and numerical results of final flow distances of three mortars. **Fig. 12** shows the errors of SPH and MPS simulations. The error was a ratio of the difference between numerical result and experimental result to experimental results. SPH/SPH-B and MPS/MPS-B represent the numerical results of flow distance at the flow stop time (hereafter briefly called stop-flow distance), in which B represents the boundary resistance was considered.

For any of two numerical methods, the simulation results were different from whether the boundary resistance was considered or not. In case of SPH, for Series No.1, the calculation errors of stop-flow distance were reduced from 73.7% to 40.8%, when considering the boundary resistance. For Series No.2 and No.3, although the flow distance was reduced after considering the boundary resistance, the flow did not stop, as shown in **Fig. 10** (No.2 and No.3). The consideration of boundary resistance had a little effect on the calculation accuracy of flow simulation. This is because the repulsive force of boundary increases as the flow rate increases. The flow of Series No.2 and No.3 was faster than Series No.1. The repulsive force of boundary makes the fluid particles in SPH to not close to the boundary so that the boundary resistance reduced.

In case of MPS, if considering the boundary resistance, the flow eventually stopped with the combined action of viscous force and boundary resistance. The simulation errors of stop-flow distance were smaller than 5 % for high fluidity samples. This means the proposed boundary resistance model can accurately reflect the

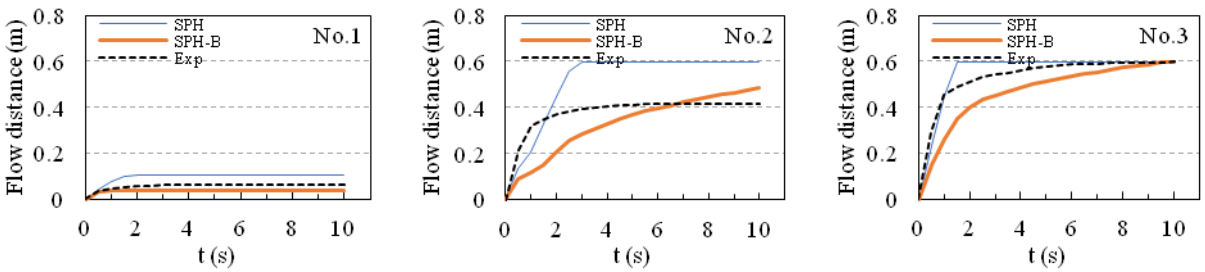

Fig. 10 Comparison of SPH results with experimental results

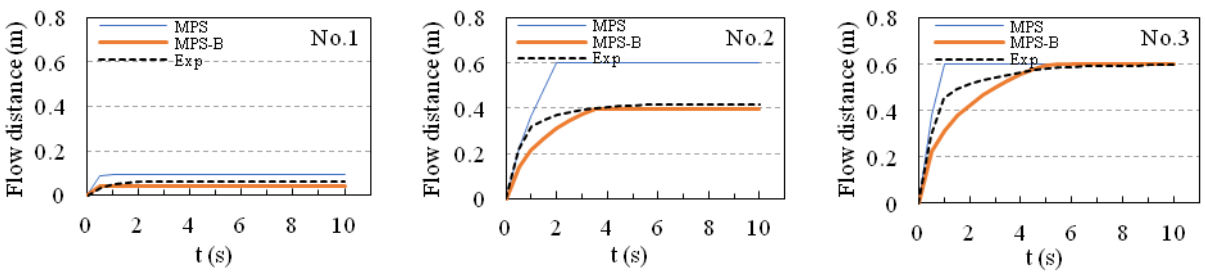

Fig. 11 Comparison of MPS results with experimental results

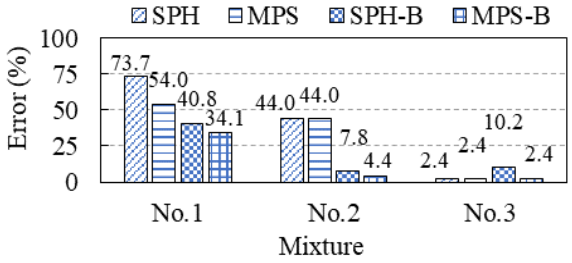

Fig. 12 Calculation errors of stop-flow distance

influence of boundary on mortar's flow. However, for Series 3 that had high fluidity, there was no great difference in flow distance between the numerical and experimental results after 5.0 seconds, no matter whether the boundary resistance was considered or not, as shown in **Fig. 10** (No.3). Hence, for high fluidity mortar, even if the boundary resistance is unclear, the MPS simulation may give an accurate result.

6.3.2 Influence of mixture's fluidity on the difference of calculation accuracy

The flow rate is the slope of flow distance-time relational curve at a certain time point. In case of considering the boundary resistance, the SPH numerical flow rate of No.2 and No.3 are not close to 0 at the stop of flow or at 10 seconds. As mentioned above, due to the effect of boundary resistance, SPH is more weakened for high fluidity samples. The numerical flow of Series No.2 lasts even after 10 seconds. The numerical flow of Series No.3 does not stop neither if the horizontal part of L-box is not limited in length. Because of this reason, the trend that the error decreases with the increase of fluidity, shown in **Fig. 13**, does not mean that SPH is applied to high fluidity cement mortars.

For MPS, in the flow deceleration phase, as the effective viscosity of mortar, calculated by regularized Bingham model, was much higher than its real viscosity, as shown in **Fig. 1**, the stop of numerical flow is earlier than the experiment. But since the final flow distance is dependent on yield stress, the calculation result of final flow distance is not affected by the effective viscosity. The final flow distance is well consistent with the experimental results, as shown in **Fig. 11**.

Fig. 13 indicates the calculation errors of stop-flow distance in case of considering the boundary resistance. The errors between the SPH's results and the experimental results are 40.8%, 7.8% and 7.7% for Series No.1, No.2, No.3, respectively. Despite the errors of Series No.2 and No.3 are smaller than that of Series No.1, the errors will increase if the computation continues and the flow distance is not limited. On the opposite, the simulation results of MPS are in agreement with the experimental results, not depending on the fluidity of mortar. The error is even less than 5% for No.2 and No.3.

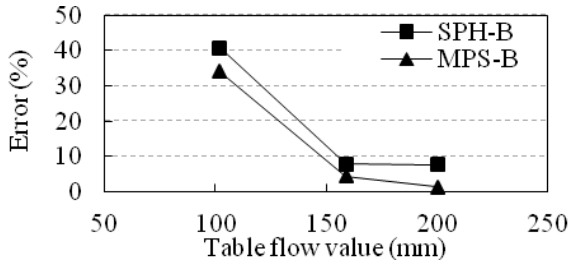

Fig. 13 Effect of fluidity on calculation error of stop-flow distance

7. CONCLUSIONS

In this study, we compared the calculation time and accuracy of weakly compressible SPH and MPS methods for fresh mortars. Main conclusions are as follows:

(1) Time-step extremely affects calculation time of flow simulation. MPS can use short step time, thus it has higher efficiency than SPH.
(2) The boundary slippage resistance has a great influence on the simulation results especially for the mortars having low fluidity. If the mortars have high fluidity, this influence becomes very smaller in SPH.
(3) SPH is more suitable for the numerical flow simulation of fresh mortar with low fluidity, whereas MPS is of wide application, provided that the boundary slippage resistance is exactly considered.
(4) For the flow simulation of fresh mortars, the MPS method has higher accuracy than the SPH method.

REFERENCES

[1] L. B. Lucy, "A Numerical Approach to the Testing of the Fission Hypothesis," *Astron. J.*, 1977.

[2] J. J. Monaghan, "Simulating Free Surface Flows with SPH," *J. Comput. Phys.*, vol. 110, no. 2, pp. 399–406, Feb. 1994.

[3] S. Koshizuka and Y. Oka, "Moving-Particle Semi-Implicit Method for Fragmentation of Incompressible Fluid," *Nucl. Sci. Eng.*, vol. 123, no. 3, pp. 421–434, Jul. 1996.

[4] R. Deeb, S. Kulasegaram, and B. L. Karihaloo, "3D Modelling of the Flow of Self-compacting Concrete with or without Steel Fibres. Part I: Slump Flow Test," *Computational Particle Mechanics*, vol. 1, no. 4. pp. 373–389, 2014.

[5] H. Lashkarbolouk, M. R. Chamani, A. M. Halabian, and A. R. Pishehvar, "Viscosity Evaluation of SCC Based on Flow Simulation in the L-box Test," *Mag. Concr. Res.*, 2013.

[6] G. Cao and Z. Li, "Numerical Flow Simulation of Fresh Concrete with Viscous Granular Material Model and Smoothed Particle Hydrodynamics," *Cem. Concr. Res.*, vol. 100, pp. 263–274, Oct. 2017.

[7] J. MURATA and K. SUZUKI, "Study on Grout Flow in Pipe with Sliding at Wall.," *Doboku Gakkai Ronbunshu*, vol. 1987, no. 384, pp. 129–136, Aug. 1987.

[8] H. Zhu, N. S. Martys, C. Ferraris, and D. De Kee, "A Numerical Study of the Flow of Bingham-like Fluids in Two-dimensional Vane and Cylinder Rheometers Using a Smoothed Particle Hydrodynamics (SPH) Based Method," *J. Nonnewton. Fluid Mech.*, vol. 165, no. 7–8, pp. 362–375, Apr. 2010.